SS-48
2023
2024

LARGE MOMENTUM TRANSFER INELASTIC MUON SCATTERING AT NAL

L. N. Hand
Cornell University

ABSTRACT

Experiments to measure the deep inelastic scattering of 100-GeV muons are considered. Both single-arm (Stage I) and coincidence (Stage II) experiments look feasible, using a torodial iron spectrometer and detecting scattered muons between 60 mrad and 150 mrad. Background from pion decays is minimized by maximizing the muon transverse momentum. For muon beams of 10^7/sec rates of 70/hr (Stage I) and 8/hr (Stage II) are expected without serious problems at momentum transfers between 20 and 80 $(GeV/c)^2$.

The Stage I experiment is of great interest and appears practical for an early stage of machine operation since it is both simple and relatively inexpensive.

I. INTRODUCTORY REMARKS

Recent data on deep inelastic electron scattering taken at SLAC (Fig. 1) has led to the exciting discovery that the cross section appears to be a slowly varying function of only one variable: ν/q^2 (q^2 = four momentum transfer, ν = energy loss of the incident electron). A great deal of theoretical speculation[1,2] has been stimulated by this, all of which is still in a somewhat primitive state without a clear picture having emerged. The "scaling law" (ν/q^2 dependence) is thought[3] to be related to the existence of singularities in the commutators of the electromagnetic current near the light cone, while the slow varies as a function of q^2 reveals an apparent point-like structure suggestive of the "parton" model which ascribes a granular charge distribution to the proton.

The intuitive picture we are offered is that inelastic scattering measures an instantaneous charge distribution, rather than a time average as measured by elastic scattering--hence the inelastic scattering enables us to examine the internal structure of the proton in more detail.

With muons, and possibly with electrons, NAL can significantly broaden our experimental range in momentum transfer (q^2) and ν (energy loss of the incident muon or electron). A better separation of σ_T and σ_L can be made over a wide range

of q^2 and ν at NAL. SLAC data are confined to $q^2 < 2.5$ (BeV)^2 and $\nu \lesssim 7$ BeV. With the beams available at NAL measurements at $q^2 \gtrsim 25$ (BeV)^2 and $\nu \leq$ 50-60 BeV can be obtained. The search for structure effects (q^2 dependence) and "scaling law" tests will move into an entirely new kinematic region one order of magnitude higher than that available to SLAC. Perhaps even more important, the duty cycle at NAL permits observation of the reaction products, about which there is no information at present owing to the low duty cycle at SLAC and the backgrounds associated with electron machines.

II. EXPERIMENT ON DEEP INELASTIC SCATTERING

Below we discuss an experiment to measure the deep inelastic scattering of 100-BeV muons. The experiment can proceed in stages, beginning as a "single-arm" experiment in which one measures W_2 (q^2, ν), observing only the scattered muons. This can be done relatively cheaply and simply, and is a prerequisite to any more elaborate detection of the reaction secondaries (except the muon). Such a second stage requires a large magnet and more elaborate spark chamber-counter system. It would seem wise to postpone the second stage until after some experience had been gained with the beam and the scattered muons.

Many authors, notably Perl (National Accelerator Laboratory 1968 Summer Study report) and R. Wilson (1968 National Accelerator Laboratory Summer Study report) have discussed inelastic muon scattering at NAL, and it is useful to delineate the different emphasis of this report from theirs:

1. Here we design for high q^2 and large ν. Excluding low q^2 greatly simplifies the experiment and the data handling. Beam halo problems become less severe.

2. Perl uses beams $\approx 10^5$ μ/sec. We design around the available intensity of $\geq 10^7$ μ/burst and avoid the problems which might arise from such intensity by observing, at least in the first stage experiment, relatively large scattering angles, $\theta_{\mu'} > 60$ mrad. In using this higher intensity we hope to take advantage of the experience soon to be gained at the AGS at 10^7 μ/sec. We note that NAL has a duty cycle 500 times that available at SLAC and that in terms of instantaneous rates 2×10^4 μ/sec at SLAC is the same as 10^7 μ/sec at NAL.

3. Perl discusses the separation of longitudinal and transverse cross sections using muons of variable incident energy and scattering angle. We plan, initially at least, to fix both the incident energy (100 GeV) and the muon scattering angle (60-150 mrad). This simplifies the experiment further, but excludes low q^2 and thus an investigation of the connection between electroproduction (muoproduction ?) and photoproduction, i.e., an extrapolation to $q^2 = 0$. It is better to make a clear distinction in the design of any experiment about which type of information is being sought. All

presently published muon inelastic experiments[4-6] belong to the category discussed by Perl (low $q^2 < 1$ GeV) and not to the type discussed here. Of course these are different kinematic limits of the same reaction.

III. SINGLE-ARM HIGH q^2 EXPERIMENT (MUONS)

A. Geometry, Counters, Spark Chambers

Figure 2 shows the experimental geometry for the Stage I single-arm muon experiment. The beam[7] is assumed to be:

100 ± 5 GeV/c muons at 10^7 muons/burst

π/μ ratio $< 10^{-5}$

$<$ 30 cm diam

$<$ 1 mrad divergence.

A hydrogen/deuterium target (for comparison with the ν experiment,[8] a high-Z target is also used) 1 meter long and 30 cm in diameter is placed in the beam 8 meters upstream of a magnetized iron toroid similar to the type discussed by Frisch.[9] All muons with scattering angles between 60 and 150 mrad pass through the magnetized iron and are given a transverse momentum of 2.5 ± 0.26 BeV/c by the azimuthally oriented B field in the iron (± 0.26 BeV/c is the uncertainty due to multiple scattering in 5 meters of iron; the field in the iron is 16 kG). The ionization energy loss (assuming 2.7 MeV/g/cm^2 and $\rho_{Fe} = 7.8$ g/cm^2) is 10.5 BeV, producing a cutoff in the minimum observable final muon energy at 11 BeV.* Track location at 2 intermediate points in the spectrometer helps with the reconstruction of secondary muon momenta. In practice, one fits to the hypothesis that a muon traversed the iron being scattered by multiple scattering and losing energy at a rate corresponding to $\overline{dE}/dx$ in iron. For a 20 microbarn cross section, the interaction probability is about 5% and a correction of about this magnitude will have to be made. Beam muons of lower momentum can be put through the apparatus and thus used to generate an empirical correction procedure. In the rate calculation given below, I have assumed

$$E'_{min} \sim 1/2\, E'_{max}$$

$$\sim 40 \text{ GeV at } 60 \text{ mrad}$$

$$\sim 15 \text{ GeV at } 150 \text{ mrad.}$$

Halo counters are used upstream of the target, since this particular trigger is sensitive to the presence of beam halo. The counter arrangement shown includes:

---

*The effect of Landau straggling on the momentum resolution dictates raising the lower cutoff to $\approx$ 20 BeV.

1. Halo counters: (V_a) 4 m×4 m o.d., $(0.3\ m)^2$ hole.

2. Beam defining counters, including momentum definition to 10%: $S_1\ S_2\ S_3 \cdot S_1\text{-}S_3$ are 10 counter hodoscopes with 3×30 cm scintillators.

3. A beam veto in the unscattered beam (V_b). This counter is placed far downstream and designed so that μ-e scattering events (which always give either μ or e inside a 3.2 mrad cone) count in V_b.

4. Trigger counters T_1-T_4. These are large liquid scintillators (liquid is cheapest for large counters) which roughly define the muon trajectory through the iron spectrometer. The o.d. of the largest of these counters is 2 meters (T_4). Each of the T's is actually 6 large counters corresponding to the hexagonal geometry of the spectrometer.

We note the size of the veto counter is determined by the beam size. The length of the hydrogen target and the distance to the spectrometer are dictated primarily by Stage II geometric requirements and a longer target could be used in Stage I. The length of the iron comes from the transverse momentum requirement and the E'_{min} cutoff from ionization loss. Lateral spreading from the ideal trajectory through the iron is caused by multiple scattering and fluctuation in dE/dx. We estimate the former as:

$$\Delta R \approx (1/3)\ 5\ \text{meters}\ \langle \theta^2_{rms} \rangle^{1/2}$$

$$\approx 1.7\ \text{m} \times \frac{0.26}{p} \simeq \frac{44\ \text{cm}}{p\ \text{BeV}} < \pm 3\ \text{cm (rms)}.$$

This seems well matched (in fact a bit small) to the transverse dimensions of the iron. If only the single-arm experiment is to be done and a beam of diameter < 30 cm is available, a smaller iron spectrometer might be used. The trigger requirement is:

$$(S_1 \cdot S_2 \cdot S_3) \cdot (T_1 \cdot T_2 \cdot T_3 \cdot T_4) \cdot (\overline{V_a + V_b}).$$

The use of a hodoscope serves the dual function of insuring the high initial momentum of the interaction and helping $(S_2 \cdot S_3)$ with the reconstruction of the beam muon in the Charpak chamber placed in the beam. The beam veto reduces the possibility of accidentals with horizontal cosmic-ray muons or between a high energy-low energy pair of muons in the beam. Depending on the beam quality, etc., some of these counters (e.g., S_1) might prove unnecessary, but a conservative design should include them.

Four x and y Charpak chambers are placed immediately before and after the target. We determine, with moderate precision, (~1 mrad), the angle of the primary

and secondary muons. The S_1 hodoscope lies upstream of the last bending magnet in the muon beam which we are assuming has at least two bends. $S_1 \cdot S_2 \cdot S_3$ should be a fast coincidence (several nanoseconds) to reduce beam accidentals to a few percent. Twenty-four conventional magnetostrictive chambers (six per plane) are installed in the spectrometer and just afterwards to obtain the secondary muon position and angle after the iron ($< \pm 3$ mrad). Care should be taken to keep the gaps within the iron small to reduce the position error resulting from delta rays accompanying the muon. The use of Charpak chambers in front is dictated by the high rates and the advantage of better handling of multiple tracks due to possible reaction secondaries.

B. Choice of Scattering Angle, Rates

Figure 3 shows the important kinematical features for the scattering of 100-BeV muons. There is a maximum possible transverse momentum p_T and secondary muon energy E' possible at a given scattering angle (θ). This maximum is achieved for elastic scattering and all other muons have less than the maximum E'. The kinematics of elastic scattering are:

$$q^2 = 2EE'(1 - \cos\theta)$$

$$\nu = E - E'$$

k = "equivalent proton energy" = $\nu - q^2/2M$ (M = proton mass). k is related to the c.m. energy in the hadron-visual photon system: $E^* = \sqrt{2kM + M^2}$

$$E' = \left(1 - \frac{k}{E}\right) \frac{E}{1 + \frac{E}{M}(1 - \cos\theta)} \qquad (k = 0 \text{ for elastic scattering})$$

p_T (max) at $\theta \sim \sqrt{2M/E} \sim 140$ mrad for E = 100 BeV

$\approx (1 - k/E)$ 7 BeV/c.

We see that the existence of a maximum in the transverse momentum of the muon for a given k suggests that $\theta \sim 140$ mrad forms a natural optimum scattering angle where backgrounds from $q^2 \approx 0$ muon inelastic scattering* are minimized. An upper bound to the observable k will be determined by the rate at which muon-produced pions (or pions from the beam contamination) decay into muons which appear as false secondaries. Since these background muons derive from pions presumably distributed as $e^{-p_\perp^2/(0.35)^2}$, the requirement $p_\perp > 2.3$ BeV/c ($k < 2/3\ E \approx 60$ BeV) should strongly suppress these events relative to the real secondaries. The use of a beam veto should also help reject these background events. Finally, a correction can be applied by

*Pions can be produced which simulate muons by decay in flight before the spectrometer.

subtracting muons of the same sign with reversed beam sign (assuming one-photon exchange is valid for the q^2 background events, and no π contamination). Thus, the observed counts (B_+ = background of μ^+, S, S' = signal) are given in the following table:

Beam	Detected Muon	
	μ^+	μ^-
μ^+	$B_+ + S$	B_-
μ^-	B_+	$B_- + S'$

Thus, we can check one-photon exchange (S' = S) for the deep inelastic process. This is important to help rule out the possibility of "pathological" muon-proton interactions at these high energies.

The maximum angle, 150 mrad, was chosen small enough to maintain the high energy of the secondary muon, keeping in mind the ionization loss in the iron spectrometer. In terms of checking the Rosenbluth formula $\cot^2 \theta/2$ is the relevant parameter. This varies from ≈ 1100 to 178 over the θ range covered. For separation of σ_L and σ_T (see Perl's report) we compare this to $q^2/2M^2\,(1 + \nu^2/q^2) \approx \nu^2/2M^2$ and find we might be sensitive over some part of the range to variations in σ_T/σ_L. The virtual photons are essentially 90-100% linearly polarized[10] in the production; angular correlations with respect to the direction of the momentum transfer will be of great interest in Stage II. We can look for cos θ terms (T-L interference) and cos 2 θ terms (T-T interference), hopefully yielding a rich store of information about production mechanisms at high q^2.

From the SLAC electron scattering $W_2 \approx 0.3/\nu$. The correspondence between this and the cross sections is predicted by the formula obtained at low q^2 by Wilson:[4]

$$q^2 > 0.7 \qquad \nu > 1.5 \qquad \left.\frac{d^2\sigma}{d\Omega\, dE'}\right|_{SLAC} = \frac{\alpha^2}{4E^2}\,\frac{\cos^2\frac{\theta}{2}}{\sin^4\frac{\theta}{2}}\,\frac{0.3}{\nu}\,.$$

(The full formula[11] in terms of W_1 and W_2 or σ_T and σ_L is given for completeness--here we assume $W_1 << W_2$.)

$$\frac{d^2\sigma}{d\Omega\, dE'} = \frac{\alpha^2}{4E^2 \sin^4\frac{\theta}{2}}\left(W_2 \cos^2\frac{\theta}{2} + 2W_1 \sin\frac{2\theta}{2}\right)$$

$$W_2 = \frac{k}{4\alpha\pi^2} \frac{\sigma_L + \sigma_T}{1 + \nu^2/q^2}$$

$$\frac{W_1}{W_2} = \left(1 + \frac{\nu^2}{q^2}\right)\left(\frac{\sigma_T}{\sigma_T + \sigma_L}\right).$$

R. Wilson quotes a formula derived from 12-BeV muon scattering at low q^2:

$$(\sigma_L + \sigma_T)_{\text{Wilson}} = \frac{135 \pm 16\ \mu b}{1 + q^2\ (2.5 \pm 0.3)}.$$

Here we have divided Wilson's quoted carbon cross section by 12. Wilson's formula gives:

$$W_2 = \frac{k}{4\alpha\pi^2}\left(\frac{\sigma_T + \sigma_L}{400\ \mu b}\right) \frac{1}{1 + \nu^2/q^2}.$$

Substituting Wilson's expression in the SLAC limit:

$$\frac{\nu^2}{q^2} >> 1 \quad \nu > \frac{q^2}{2M}$$

$$W_2 \approx \left(\frac{135 \pm 16\ \mu b}{400\ \mu b}\right) \frac{1}{4\alpha\pi^2} \frac{1}{2.5 \pm 0.3} \frac{1}{\nu}$$

$$\approx \frac{0.47 \pm 0.1}{\nu}.$$

We note this is high by 50% if we extrapolate to the SLAC limit. This probably expresses the inadequacies of the fit and not a discrepancy between muon and electron inelastic scattering. We use $0.3/\nu = W_2$ for our estimate of rates.

Integrating for fixed ν from 60-150 mrad and over 2π in azimuth, we obtain

$$2\pi \int_{\theta_{\min}}^{\theta_{\max}} \sin\theta\ d\theta\ \frac{d^2\sigma}{d\Omega\, dE'} = \frac{\alpha^2}{4E^2} \frac{0.3}{\nu} 4\pi \left(\frac{1}{y^2} - 2\log y\right)_{y_{\min}}^{y_{\max}}$$

$$= 5\times10^{-37} \frac{3.6}{\nu} 1.1\times10^3,$$

where

$$y \equiv \sin \frac{\theta}{2}$$

$$\frac{d\sigma}{d\nu} = \frac{2nb}{\nu}.$$

If we integrate $\int d\nu \; d\sigma/d\nu$ over a range in ν of a factor of e, we obtain 2 nb. The final numbers are

$\Delta\Omega = 57$ msr $\qquad 60_{mrad} < \theta < 150$ mrad

$\sigma_{eff} = 2$ nb $\qquad 0 < \phi < 2\pi$

$= 20 \times 10^{-34} cm^2 \qquad \int \frac{d\nu}{\nu} = 1$

EVENTS/10^7 MUONS = 8 10^{-2} (40 in. LH_2)

EVENTS/HOUR ≃ 70

C. Backgrounds

The background of secondary muons from π decay is estimated thus:

Rate ($\mu \rightarrow n\pi$; $\pi \rightarrow \mu$) =
[Total μ interaction rate ($\nu > 80$ BeV)]
× (π multiplicity) × (decay probability for a 20-BeV π in 8 meters)
× (S).

These factors are

1. $\sigma(\mu p;\ \nu > 80) \approx 3.5$ μb
2. π multiplicity ≈ 5
3. decay probability ≈ 0.6%.

The effective cross section is then 0.1S μb where S is a suppression factor from the requirement of high p_T. If the distribution is $\sim e^{-p_T^2/(0.35)^2}$, then we expect e^{-100} for $p_T \geq 2.3$ GeV. A better estimate would be to assume $S \approx d\sigma/dt|_{t=p_\perp^2} \; |d\sigma/dt|_{t=0}$ for πp or pp scattering. This gives[12] $S < 10^{-6}$. In either case, this background is negligible compared to 2 nb. The above estimate predicts a contamination of less than 0.1% for $p_T > 2.3$ GeV. The requirement of large p_T is the reason for the elimination of π decay as a background.

IV. COINCIDENCE EXPERIMENT: STAGE II

Figure 4 shows the proposed geometry for a coincidence experiment to observe the reaction products. A large magnet similar to the 120D36 now in use at

Brookhaven, but twice as long, is placed longitudinally along the beam with the center of the beam 0.5 m from the pole edge. With this geometry very high momentum secondary particles traverse a greater length of magnetic field than those of low momentum and $\Delta p/p \sim$ constant instead of $\sim p$ as is usually the case. Of course we depend here on the high-energy particles being collimated more forward. The figure shows the range of angles for the 3-momentum transfer of $\vec{q}$. We see that the forward direction for the reaction secondaries can be as much as 15° to one side.

By surrounding the magnet with (optical) spark chambers on both sides of the target we can obtain almost full coverage. Wide gap chambers (2 in. gap) are easy to construct and have the property of supporting multiple tracks. Slow tracks in the backward direction can be momentum analyzed in the magnet fringe field which should be appreciable even 1 meter from the 1 meter gap at the magnet. The iron muon spectrometer is only operated over 1/6 of its solid angle to match the azimuthal range of $\vec{q}$ into the large air gap magnet. We roughly estimate the rate at ~ 10% of the single arm rate, or about 8/hour. Each wide gap chamber on the outside of the experiment has a second section separated from the first by 2 r.ℓ. of lead to convert gamma rays from the π^0's. Recoil protons from some of the reactions might be identified by dE/dx counters and by ionization in the wide gap chambers. Vidicon readout[13] might prove useful and cheap due to the size and the lack of extreme requirements of precision on track measurement. The wire chambers on the muon side would help sort the reaction data by q^2 and ν.

In designing the geometry for the secondary detector it is difficult, due to the extreme generality of the device, to make specific statements. Here we have compromised between the cost of a large magnet and the general features of the reaction kinematics.

Specifically the kinematics are

$$0.04 < \theta_{\vec{q}} \ (60 \text{ mrad} = \theta_{\mu}) < 0.25$$

$$\frac{1}{\gamma_{cm}} \approx \frac{1}{6}.$$

This means that the reaction products tend to come out in a cone of half angle 1/6 centered about θ_q. This magnet roughly matches this geometry. Other particles are of low energy and do not need one. The central field is assumed to be 8 kG. The fringe field, even for the scattered muon, should produce a deflection of about 7 mrad for 100-GeV beam muons and make possible an additional measurement of the secondary muon momentum. We note the lack of dependence of γ_{cm} on q^2, ν appears to be a happy accident since:

$$\gamma_{cm} \approx \frac{\nu}{k}\sqrt{\frac{k}{2M}} \qquad \nu \to k\,q^2 \to 0$$

$$\gamma_{cm} \to \sqrt{\frac{k}{2M}}$$

For "missing" mass studies using the recoil proton, we of course have relatively poor mass resolution in the reaction:

$$q_0 \text{ (virtual photon)} + \underline{p} \to \underline{p} + X$$

$$t_{min} \simeq \left(\frac{q^2 + M_X^2}{2\nu}\right)^2$$

$$t_{min}(q^2) > t_{min}(0).$$

We see the resolution is poor for $M_X^2 < q^2$ if we look at the recoil proton.

Quantities of interest which might come out of such a study:

1. $\sigma_{(\rho^o)}/\sigma_{TOT}$ vs (q^2, ν), checks of vector dominance at high q^2, search for heavy vector bosons (maybe more prominent at large q^2).

2. t distribution of recoil protons vs q^2, ν, missing mass.

3. Fraction of the time strange particles are produced (K_S and Λ are detected by V's).

4. Multiplicity of charged and neutral particles produced in the final state vs q^2, ν. Statistical distribution of p_L and $p_\perp$ for reaction secondaries.

5. Polarization correlation information about reaction secondaries. This probably requires much better statistics than will be available since one must look at particular reaction channels.

Rough Cost Estimate for the Magnets

We first estimate the volume of the Stage I muon detector considered as a truncated cone 5 meters high with a 2 meter base radius and a 1.2 meter top radius as 42 m^3 (370 tons). Using a cost figure of \$300/ton for good quality machined iron we arrive at a cost of \$110 K for the muon magnet. If we do not cover the full azimuthal range an even cheaper magnet can be designed.

To estimate the cost of the Stage II magnet is harder. The iron must have at least a 2 m return leg to avoid saturation and thus the total iron is $\approx$ 36 m^3 or $\approx$ \$100 K. To estimate the copper we observe the number of ampere turns must be 7×10^5 to produce 8 kG across a 1 meter gap. A design current density of 700 A/cm^2 would mean a cross sectional area of 10^3 cm^2 for the coil. With the size of the magnet

given, this implies a copper volume ≈ 1.5×10^6 cm^3 or 14.5 tons of copper. At \$5/lb in the finished coil, this implies a coil cost (finished coil) of \$140 K, giving a total magnet cost of \$240 K. The power requirement is estimated to be 1.25 MW for 8 kG in the gap.

Thus we see that, exclusive of setting up the beam, we could expect to do Stage I for ≈ \$250 K and Stage II for an additional \$350 K. Here we have added to the cost of the magnet to cover the cost of the spark chambers, counters, electronics, etc. This would seem a reasonable cost for what may prove to be one of the exciting pieces of physics to emerge from the 200-GeV accelerator.

We conclude that this is an extremely important experiment which seems quite practical to do at an early stage of operation and at a moderate cost.

The equivalent electron experiment appears possible, although much more difficult. Electron beams have a thousand times worse pion contamination and are about a factor of 3 lower in intensity. Dalitz pairs from π^0 decay cause severe backgrounds.

REFERENCES

[1] E. A. Paschos, Theoretical Ideas on Inelastic Electron-Nucleon Scattering, talk presented at the 1969 Boulder Conference on High Energy Physics.

[2] J. D. Bjorken, Phys. Rev. 179, 1547 (1969); R. P. Feynman, (unpublished). H. D. Abarbanel, M. L. Goldberger, and S. Treiman, Phys. Rev. Letters 22, 500 (1969); H. Harari, Phys. Rev. Letters 22, 1078 (1969).

[3] For a general review of this subject, see L. S. Brown, Causality in Electroproduction at High Energy, to be published.

[4] C. M. Hoffman et al., Phys. Rev. Letters 22, 659 (1969).

[5] B. D. Dieterle et al., Phys. Rev. Letters 23, 1187 (1969).

[6] W. T. Toner, Proc. International Conference on High Energy Electron and Photon Interactions, Liverpool, 1969.

[7] Recent work on the design of NAL muon beams: T. Yamanouchi, A Muon Beam at NAL, National Accelerator Laboratory 1968 Summer Study Report B.2-68-38, Vol. II, p. 1; T. Kirk, Long Spill Muon and Neutrino Beams in Area 1, National Accelerator Laboratory 1969 Summer Study Report SS-43, Vol. I; L. C. Teng, Possible Layouts for a Muon-Long Spill Neutrino (μ-ν_L) Beam, National Accelerator Laboratory 1969 Summer Study Report SS-64, Vol. I; J. H. Christenson, Some Simple Muon Beams, National Accelerator Laboratory 1969 Summer Study Report SS-96, Vol. I.

[8] L. N. Hand, A Study of 40-90 GeV Neutrino Interactions Using a Tagged Neutrino Beam, National Accelerator Laboratory 1969 Summer Study Report SS-151, Vol. I.

[9]D. Frisch, private communication.

[10]L. Hand and R. Wilson, SLAC-25 (1963).

[11]S. D. Drell and J. D. Walecka, Ann. Phys. (N. Y.) 28, 18 (1964).

[12]Proc. International Conference on High Energy Physics, Vienna, 1968, p. 330.

[13]A. Roberts, Wire Arrays vs Vidicons: A Comparison of Large Wire Arrays with Optical Spark Chambers Using Vidicon Readout, National Accelerator Laboratory 1969 Summer Study Report SS-56, Vol. III.

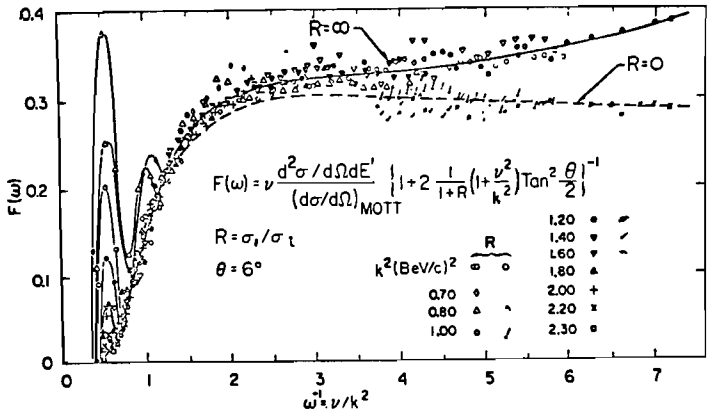

Fig. 1. Experimental results from SLAC inelastic electron scattering, plotted to show "scaling law" validity. $F(w) = \nu W_2$ (taken from the talk by W. K. H. Panofsky in Proceedings of the 14th International Conference on High Energy Physics, Vienna, 1968.

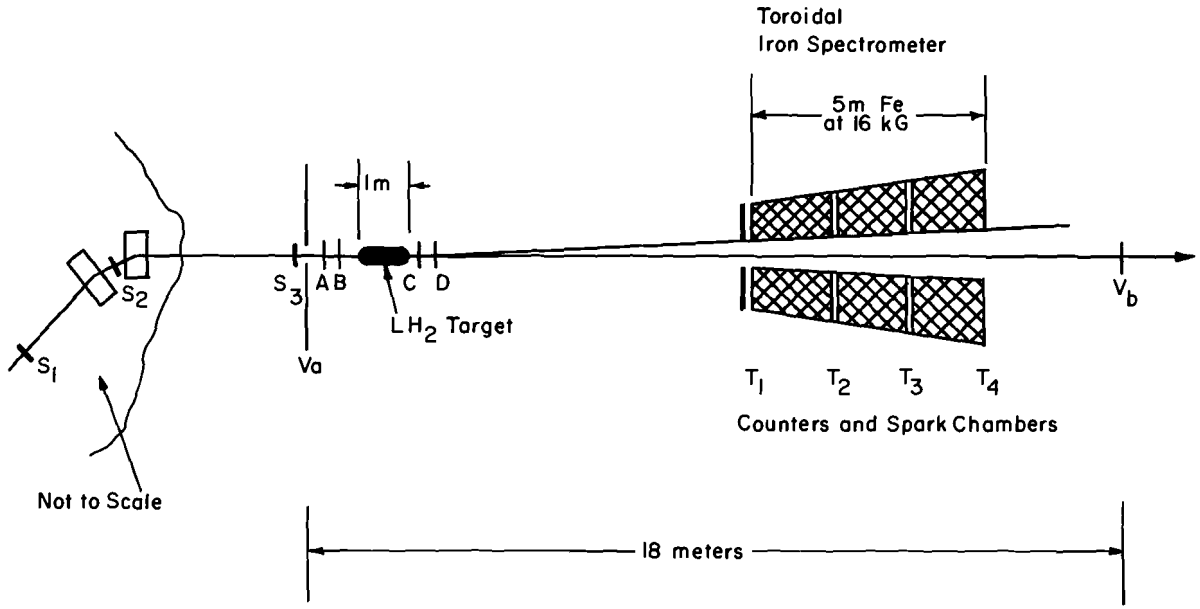

Fig. 2. Stage 1 single-arm muon inelastic scattering experiment. A, B, C, and D are proportional chambers; beam diameter is 30 cm.

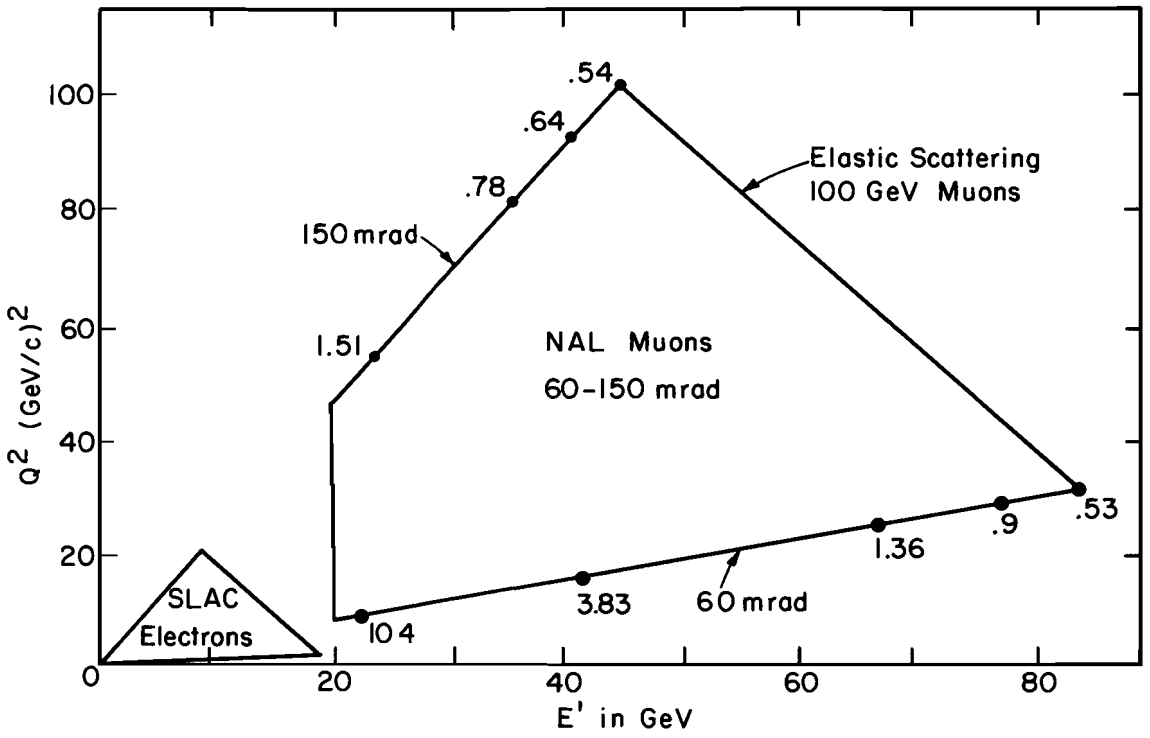

Fig. 3. Kinematic region in q^2 and ν available to NAL compared to that available at SLAC. We assume: 60 mrad $< \theta_\mu <$ 150 mrad. Dots along boundaries refer to values of $w^{-1} = \nu/q^2$.

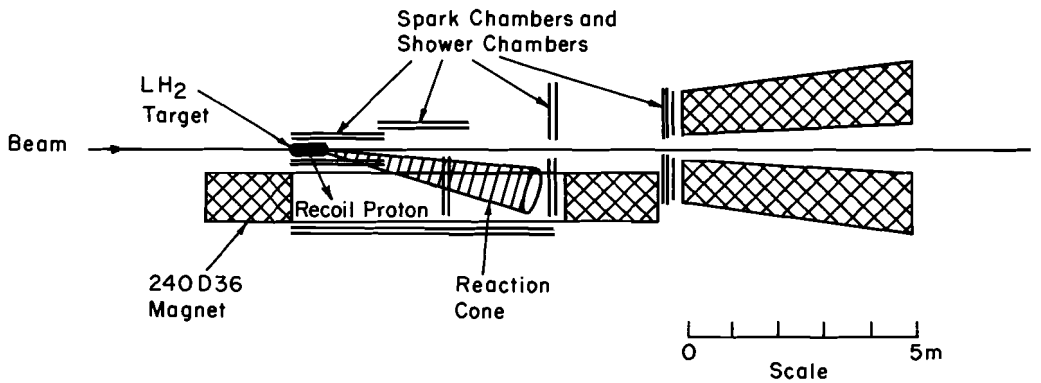

Fig. 4. Stage II--coincidence experiment.